

Non-Markovian behaviour and the dual role of astrocytes in Alzheimer's disease development and propagation

Swadesh Pal^{a,*}, Roderick Melnik^{a,b}

^a*MS2 Discovery Interdisciplinary Research Institute, Wilfrid Laurier University, Waterloo, Canada*

^b*BCAM - Basque Center for Applied Mathematics, E-48009, Bilbao, Spain*

Abstract

Alzheimer's disease (AD) is a common neurodegenerative disorder nowadays. Amyloid-beta ($A\beta$) and tau proteins are among the main contributor to the development or propagation of AD. In AD, $A\beta$ proteins clump together to form plaques and disrupt cell functions. On the other hand, the abnormal chemical change in the brain helps to build sticky tau tangles that block the neuron's transport system. Astrocytes generally maintain a healthy balance in the brain by clearing the $A\beta$ plaques (toxic $A\beta$). But, over-activated astrocytes release chemokines and cytokines in the presence of $A\beta$ and also react to pro-inflammatory cytokines further increasing the production of $A\beta$. In this paper, we construct a mathematical model that can capture astrocytes' dual behaviour. Furthermore, we reveal that the disease propagation does not depend only on the current time instance; rather, it depends on the disease's earlier status, called the "memory effect". We consider a fractional order network mathematical model to capture the influence of such memory effect on AD propagation. We have integrated brain connectome data in the network model and studied the memory effect and the dual role of astrocytes together. Depending on toxic loads in the brain, we have also analyzed the neuronal damage in the brain. Based on the pathology, primary, secondary, and mixed tauopathies parameters have been used in the model. Due to the mixed tauopathy, different brain nodes or regions in the brain connectome accumulate different toxic concentrations of toxic $A\beta$ and toxic tau proteins. Finally, we explain how the memory effect can slow down the propagation of such toxic proteins in the brain and hence decreases the rate of neuronal damage.

Keywords: Neurodegenerative disorders, Alzheimer's disease, Astrocytes, Fractional differential equations, Neuroglia and astroglia, Multiscale modelling, Non-Markovian process, Caputo fractional derivatives, Network model, Brain connectome

1. Introduction

Alzheimer's disease (AD) is a progressive and irreversible neurodegenerative disorder that affects memory, thinking, and behaviours. These cognitive declines may be so severe that to interfere with daily tasks. Dr. Alois Alzheimer first observed this disease in 1906 and described it as "a peculiar disease" [1]. He examined a woman's brain who had died of an unusual mental illness, including memory loss and language problems. He found many abnormal clumps (amyloid-beta plaques) and fiber bundle tangles (tau tangles), which are now considered as one of the main contributors to AD development [1, 2, 3]. Researchers believe

*Swadesh Pal

Email addresses: spal@wlu.ca (Swadesh Pal), rmelnik@wlu.ca (Roderick Melnik)

that they block communication between nerve cells and disrupt many processes, and it causes memory loss, difficulty in speaking and other cognitive declines.

AD is not a normal part of ageing, but the risk factor of getting the disease increases with age [4, 5]. Most AD-affected people are 65 years of age or over, but it is possible to have the disease before age 65, referred to as early-onset Alzheimer's [6]. At the early stage of the disease, the AD-affected people's memory loss is mild, but over age, they lose gradually their ability to carry on a conversation or recognition. Depending on different factors, AD-affected people can live 20 years after diagnosis, but on average, they live 8 to 10 years [7, 8]. To date, AD has no cure except for a few medications such as the aducanumab that can help to reduce the cognitive decline at the early stage of the disease [9, 10, 11]. Many researchers have been working worldwide to understand the disease in a better way and prevent it from propagation.

Accumulation of amyloid-beta (A β) in the extracellular space is often considered to be one of the main initiators of the early onset of AD [12, 13, 14, 15, 16]. This accumulation may happen due to its overproduction or the lower clearance rate [17]. A β comprises 39-43 amino acids with different biophysical states, and soluble A β ₄₀ and insoluble A β ₄₂ are the two major isoforms that have been observed in the brain. In a healthy brain, more than 90% concentration of A β is observed in the form of A β ₄₀ while less than 5% is found in the form of A β ₄₂ [18, 19, 20]. But, an AD-affected brain cannot maintain this type of healthy balance, and a higher concentration of A β ₄₂ peptide causes forming plaques and disrupts normal cell function. Another important key factor of AD is the tau protein (τ P) [21, 22]. The normal τ P forms a microtubule, and they help in transporting nutrients and other substances from one part of a nerve cell to another [23]. Due to abnormal chemical changes in the brain, the tau protein detaches from microtubules and sticks to other τ P [24, 25]. This causes the tau protein to form neurofibrillary tangles (misfolded and abnormally shaped) inside neurons and block the neuron's transport system.

Researchers have been focused on identifying the concentrations of A β and τ P at the early onset of AD. To date, the accumulation of these proteins is not yet measurable with blood tests and also can not be visualized on CT or MRI scans. The FDA-approved amyloid PET scan tracer can identify the presence of AD but cannot measure the disease progression fully, so this has been used only for clinical trials [26, 27, 28]. On the other hand, F-18 floratacupir is the first FDA-approved tau PET scan tracer, and it helps in the stage of AD neurodegeneration [29, 30]. Along with these two proteins, many other factors that influence AD development and progression. Substantial efforts have been going on to identify the disease state concerning such different factors.

Astrocytes are the largest and most numerous types of glial cells in the central nervous system (CNS) as they serve as an immunodefense to the CNS. They regulate blood flow, transfer mitochondria to neurons, and help in neuronal metabolism [31, 32, 33, 34]. Generally, activated astrocytes clear debris from the brain and protect neurons from disease [35, 36, 37, 38]. But, in the AD-affected brain, they lose to maintain a healthy balance and support in AD propagation [39]. In the early stages of AD, a sufficient amount of toxic amyloid-beta mainly disrupts this healthy balance. In this case, astrocytes can not control the ionic balance in the brain, in particular, intracellular Ca²⁺ concentrations. As a result, NADPH oxidase (NOX) is stimulated, and neuronal death happens through oxidative stress [40, 41]. Many other negative effects occur due to the over-activation of astrocytes, such as apolipoprotein E (ApoE) and the excess production of glutamate. For example, one of the neurotoxic isoforms ApoE4 of ApoE supports toxic A β deposition in the initial stage of AD development [6, 42].

One of our current work's main aspects is to analyse astrocytes' dual role before and after AD. We constructed a mathematical model incorporating the role of astrocytes in AD along with the A β and τ P interactions. Each of these proteins (A β and τ P) follows a modified heterodimer model for protein-protein interactions in the reaction kinetics with a coupling parameter between them [43]. We modify the exponen-

tial growth by logistic growth in the growth term for both the healthy proteins equation [44, 45]. We consider a logistic growth in the astrocytes equation and assume that they clear toxic amyloid beta [46, 47]. Along with these, a damage equation is considered to analyze the injury to the neurons in the brain connectome as it occurs due to the toxic loads of $A\beta$ and τP [43].

Given that a reaction-diffusion process can depend not only on the previous time instance's concentrations but also on all the earlier stages of the concentrations with some weights [48, 49, 50, 51, 52, 53], this idea is further developed in this paper. A time-fractional reaction-diffusion equation is used to analyze such processes in the AD context, which we call collectively the "memory effect". This type of memory effect has been seen in the disease progression [51, 54, 55]. In this work, we construct a time-fractional network model to describe the AD progression in the brain connectome and analyze the damage dynamics concerning the memory effect. In addition, we investigate different tauopathies (primary, secondary and mixed) for the network model in the absence and presence of memories. Furthermore, we also study the disease propagation on nodes and in brain connectome regions.

The rest of this paper is organized as follows. In Sect. 2, we formulate the temporal models for AD progression for both cases: absence and presence of memories. The equilibrium points and their stabilities for the temporal model are discussed in Sect. 3. In Sect. 4, we extend the temporal model in a subset of Euclidean space and then into the network to integrate brain connectome data. Exhaustive numerical simulation results are presented in Sect. 5 to analyze the dual role of astrocytes and the memory effect in AD progression. Finally, the conclusions and future directions are presented in Sect. 6.

2. Model Formulation

Astrocytes are the glial cells present in the central nervous system, and they have been very closely associated with the development of Alzheimer's disease (AD) in the brain [56]. To capture the dual role of astrocytes in healthy and AD-affected brains, we introduce an equation corresponding to astrocytes and modify the temporal model defined in [43, 45] as

$$\frac{du}{dt} = u(a_0 - a_1 u) - a_2 u \tilde{u}, \quad (1a)$$

$$\frac{d\tilde{u}}{dt} = -\tilde{a}_1 \tilde{u} + a_2 u \tilde{u} - \mu \tilde{u} (w - \tilde{u}), \quad (1b)$$

$$\frac{dv}{dt} = v(b_0 - b_1 v) - b_2 v \tilde{v} - b_3 \tilde{u} v \tilde{v}, \quad (1c)$$

$$\frac{d\tilde{v}}{dt} = -\tilde{b}_1 \tilde{v} + b_2 v \tilde{v} + b_3 \tilde{u} v \tilde{v}, \quad (1d)$$

$$\frac{dw}{dt} = w(c_0 - w/c_1), \quad (1e)$$

where u and \tilde{u} are the healthy and toxic densities of the protein $A\beta$ and v and \tilde{v} are the healthy and toxic densities for τP . The parameters a_0 and b_0 are the mean production rates of healthy proteins, a_1 , b_1 , \tilde{a}_1 and \tilde{b}_1 are the mean clearance rates of healthy and toxic proteins, and a_2 and b_2 represent the mean conversion rates of healthy proteins to toxic proteins. Here, the parameter b_3 represents the coupling between the two proteins $A\beta$ and τP . The variable w represents the concentration of astrocytes with c_0 as the production rate and the term $c_0 c_1$ is the saturation point. The parameter μ is responsible for the dual role of astrocytes. If $w > \tilde{u}$, then astrocytes clear the concentrations of the toxic amyloid-beta; otherwise, it helps to increase the toxic concentrations.

For any time $t > 0$, the concentration of the substances depends on the reaction terms on the right-hand side of the equation (1). This is known as the Markovian process, but in reality, these concentrations not only depend on the time instance t ; rather, they depend on some weighted average concentrations of past time interval, say $[t_p, t]$ for $t_p < t$. This is usually termed collectively as the memory effect (e.g., [49, 50, 51, 53, 55]). The distribution of the weights is proportional to some power of the length of the time interval, i.e., $(t - t_p)$, following the power law correlation function [48, 51]. Without the loss of generality, we can choose $t_p = 0$. Now, incorporating these into the mathematical model, we obtain the fractional order differential equations as

$$D_t^\alpha u = u(a_0 - a_1 u) - a_2 u \tilde{u}, \quad (2a)$$

$$D_t^\alpha \tilde{u} = -\tilde{a}_1 \tilde{u} + a_2 u \tilde{u} - \mu \tilde{u} (w - \tilde{u}), \quad (2b)$$

$$D_t^\alpha v = v(b_0 - b_1 v) - b_2 v \tilde{v} - b_3 \tilde{u} v \tilde{v}, \quad (2c)$$

$$D_t^\alpha \tilde{v} = -\tilde{b}_1 \tilde{v} + b_2 v \tilde{v} + b_3 \tilde{u} v \tilde{v}, \quad (2d)$$

$$D_t^\alpha w = w(c_0 - w/c_1), \quad (2e)$$

where $D_t^\alpha z(t)$ stands for the Caputo fractional derivative that is defined by

$$D_t^\alpha z(t) = \frac{1}{\Gamma(1-\alpha)} \int_0^t \frac{z'(s)}{(t-s)^\alpha} ds, \quad 0 < \alpha < 1,$$

and z' denotes the first order derivative of z . Here in the modified fractional differential model (2), we have excluded the case $\alpha = 1$ to incorporate the memory effect, as it corresponds to the case of no memory. We also consider the memory effect in the neuronal damage equation [43, 45] by modelling it by the following equation:

$$D_t^\alpha q = (k_1 \tilde{u} + k_2 \tilde{v} + k_3 \tilde{u} \tilde{v} + k_4 q)(1 - q). \quad (3)$$

Here, $q = 0$ signifies healthy, i.e., neurons are properly functioning, and $q = 1$ implies unhealthy or no longer functioning.

3. Analysis of the Homogeneous System

Here, we analyze the temporal dynamics of the non-fractional and fractional models. First, we describe the equilibrium points of the non-fractional model (1), and their stability behaviours. The equilibrium points of the system (1) are the time-independent solutions of (1). These can be obtained by solving the system (1) with the vanishing time-derivatives. Depending on the parameter values, the system (1) has many equilibrium points, and we calculate these numerically later on. Moreover, the stability of an equilibrium point depends on the nature of all eigenvalues of the Jacobian matrix evaluated at that point. The Jacobian matrix of the system (1) evaluated at an equilibrium point $E_* = (u_*, \tilde{u}_*, v_*, \tilde{v}_*, w_*)$ is given by

$$\mathbf{J}_* = \begin{pmatrix} a_{11} & a_{12} & 0 & 0 & 0 \\ a_{21} & a_{22} & 0 & 0 & a_{25} \\ 0 & a_{32} & a_{33} & a_{34} & 0 \\ 0 & a_{42} & a_{43} & a_{44} & 0 \\ 0 & 0 & 0 & 0 & a_{55} \end{pmatrix},$$

where $a_{11} = a_0 - 2a_1 u_* - a_2 \tilde{u}_*$, $a_{12} = -a_2 u_*$, $a_{21} = a_2 \tilde{u}_*$, $a_{22} = -\tilde{a}_1 + a_2 u_* - \mu(w_* - 2\tilde{u}_*)$, $a_{25} = -\mu \tilde{u}_*$, $a_{32} = -b_3 v_* \tilde{v}_*$, $a_{33} = b_0 - 2b_1 v_* - b_2 \tilde{v}_* - b_3 \tilde{u}_* \tilde{v}_*$, $a_{34} = -b_2 v_* - b_3 \tilde{u}_* v_*$, $a_{42} = b_3 v_* \tilde{v}_*$,

$a_{43} = b_2\tilde{v}_* + b_3\tilde{u}_*\tilde{v}_*$, $a_{44} = -\tilde{b}_1 + b_2v_* + b_3\tilde{u}_*v_*$, and $a_{55} = c_0 - 2w_*/c_1$. Now, if real parts of all the eigenvalues of \mathbf{J}_* are negative, then the equilibrium point E_* is stable; otherwise, it is unstable. The non-fractional damage equation has only one equilibrium point $q_* = 1$, which is stable. The equilibrium points for the non-fractional model are also the equilibrium points for the fractional model, but their stability behaviours are not the same for both models. For a fixed α , an equilibrium point E_* of the fractional model is stable if all the eigenvalues λ_i ($i = 1, \dots, 5$) of the Jacobian matrix \mathbf{J}_* satisfy $|\arg(\lambda_i)| > \alpha\pi/2$; otherwise, it is unstable [55].

4. Network Model for the Brain Connectome

Before going to the network model for the brain connectome, we first extend the temporal model (2) into the reaction-diffusion model in a subset of the Euclidean space. A spatio-temporal extension of the fractional model (2) in a domain Ω in the Euclidean space is

$$D_t^\alpha u = \nabla \cdot (\mathbf{D}_1 \nabla u) + u(a_0 - a_1 u) - a_2 u \tilde{u}, \quad (4a)$$

$$D_t^\alpha \tilde{u} = \nabla \cdot (\tilde{\mathbf{D}}_1 \nabla \tilde{u}) - \tilde{a}_1 \tilde{u} + a_2 u \tilde{u} - \mu \tilde{u}(w - \tilde{u}), \quad (4b)$$

$$D_t^\alpha v = \nabla \cdot (\mathbf{D}_2 \nabla v) + v(b_0 - b_1 v) - b_2 v \tilde{v} - b_3 \tilde{u} v \tilde{v}, \quad (4c)$$

$$D_t^\alpha \tilde{v} = \nabla \cdot (\tilde{\mathbf{D}}_2 \nabla \tilde{v}) - \tilde{b}_1 \tilde{v} + b_2 v \tilde{v} + b_3 \tilde{u} v \tilde{v}, \quad (4d)$$

$$D_t^\alpha w = w(c_0 - w/c_1), \quad (4e)$$

where the first term on the right-hand side in each of the first four equations incorporates the random movement of the concentrations in the domain Ω . We assume that the astrocytes' density remains homogeneous in the whole domain Ω . We consider the same damage equation (3) in this spatial extension, and hereafter the damage q also depends on the spatial location, i.e., $q(\mathbf{x}, t)$, $\mathbf{x} \in \Omega$. The astrocytes also affect the damage dynamics of the neurons, as they are implicitly involved through toxic amyloid beta.

Now, we formulate the network mathematical model corresponding to the modified model (4) for the brain connectome data [43, 45]. Suppose the network brain data is represented by a graph \mathbf{G} with V nodes and E edges. For the graph \mathbf{G} , we construct the adjacency matrix \mathbf{A} . This helps us to construct the Laplacian in the graph. We define the (i, j) ($i, j = 1, 2, 3, \dots, N$) element of the matrix \mathbf{A} as

$$A_{ij} = \frac{n_{ij}}{l_{ij}^2},$$

where n_{ij} is the mean fiber number and l_{ij}^2 is the mean length squared between the nodes i and j . Now, we define the elements of the Laplacian matrix \mathbf{L} as

$$L_{ij} = \rho(D_{ii} - A_{ij}), \quad i, j = 1, 2, 3, \dots, N,$$

where ρ is the diffusion coefficient and $D_{ii} = \sum_{j=1}^N A_{ij}$ are the elements of the diagonal weighted-degree matrix. With the help of the Laplacian matrix, we derive a network mathematical model on the graph \mathbf{G} ,

whose dynamics at each node j ($j = 1, 2, 3, \dots, N$) are given by

$$D_t^\alpha u_j = - \sum_{k=1}^N L_{jk}^u u_j + u_j(a_0 - a_1 u_j) - a_2 u_j \tilde{u}_j, \quad (5a)$$

$$D_t^\alpha \tilde{u}_j = - \sum_{k=1}^N L_{jk}^{\tilde{u}} \tilde{u}_j - \tilde{a}_1 \tilde{u}_j + a_2 u_j \tilde{u}_j - \mu \tilde{u}_j (w_j - \tilde{u}_j), \quad (5b)$$

$$D_t^\alpha v_j = - \sum_{k=1}^N L_{jk}^v v_j + v_j(b_0 - b_1 v_j) - b_2 v_j \tilde{v}_j - b_3 \tilde{u}_j v_j \tilde{v}_j, \quad (5c)$$

$$D_t^\alpha \tilde{v}_j = - \sum_{k=1}^N L_{jk}^{\tilde{v}} \tilde{v}_j - \tilde{b}_1 \tilde{v}_j + b_2 v_j \tilde{v}_j + b_3 \tilde{u}_j v_j \tilde{v}_j, \quad (5d)$$

$$D_t^\alpha w_j = w_j(c_0 - w_j/c_1), \quad (5e)$$

and the corresponding damage equation is given by the corresponding fractional differential equation

$$D_t^\alpha q_j = (k_1 \tilde{u}_j + k_2 \tilde{v}_j + k_3 \tilde{u}_j \tilde{v}_j + k_4 q_j)(1 - q_j), \quad (6)$$

with non-negative initial conditions. Here, all the equilibrium points of the homogeneous system are the homogeneous stationary steady-states for the network model (5). We find these non-homogeneous stationary steady-states numerically in the next section.

5. Results and Discussion

In this section, we focus on the numerical findings for both models (non-fractional and fractional) in the brain connectome. We collect the brain connectome data from BrainGraph.org – The network of the brain (<https://braingraph.org>). These data provide the information on a network containing a set of nodes and edges located in different brain regions. It helps us in studying the spatio-temporal behaviour in the brain via these connectome data. In these brain graph data, each node corresponds to a small area ($1-1.5\text{cm}^2$) of the gray matter, called the region of interest (ROI), and there may exist an edge connected with two nodes if a diffusion-MRI based workflow finds fibers of axons, running between those two nodes in the white matter of the brain [57, 58].

Regarding the computations, we have integrated the brain connectome data into our computational environment (Matlab) and exported the Laplacian corresponding to the real data. The considered network data contains $N = 1,015$ nodes and $V = 16,280$ edges. We use the Laplacian to find the network model's numerical solution for taking care of different scenarios, as considered later in this section. The Runge-Kutta method of order four has been used for the integration of the resulting system with $dt = 0.01$, and the obtained results have been shown to be unaltered for lesser values of this time-step. We computed the numerical results based on our code implemented in C-language, and we used Sharcnet (www.sharcnet.ca) supercomputers to run multiple jobs simultaneously, which helped us to analyze efficiently different aspects of the model.

Figure 1 depicts the weighted adjacency matrix for the considered network data. In the plot, blue to red colors represent the minimum to the maximum strength of the connection between the nodes. The brain stem region is also in the diagram in between frontal and basal ganglia, but it is not visible because it contains only one node. This diagram shows the connection between the nodes and regions in the brain

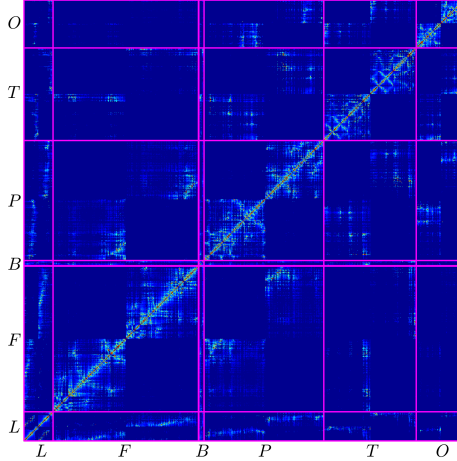


Figure 1: (Color online) Weighted adjacency matrix for the brain connectome data: limbic (L), frontal (F), basal ganglia (B), parietal (P), temporal (T) and occipital (O).

connectome. We use this matrix to find the spatio-temporal behaviour for the network model of the brain connectome. Depending on the parameter values, both models (non-fractional and fractional models) share the feasible homogeneous steady-states. In the homogeneous steady-state, the concentration corresponding to the toxic amyloid-beta may be dependent on the concentration of toxic tau protein. In this case, it is called secondary tauopathy; otherwise, it is a primary tauopathy. We discuss both cases in the coming subsection.

Before moving to the numerical simulations, we first mention the initial conditions for the variables in the network model. In the brain connectome, initial seeding sites for the toxic amyloid-beta are the temporobasal and frontomedial regions, and the toxic tau proteins are the locus coeruleus and transentorhinal associated regions. These seeding sites in the brain connectome are mentioned in [43, 45]. Here, we add small toxic loads 0.25% and 0.38% in the toxic amyloid-beta (\tilde{u}) and toxic tau protein (\tilde{v}) concentrations for the seeding sites, respectively. Due to these small perturbations, the toxic concentrations propagate all over the brain connectome and spread the AD. On the other hand, we consider healthy concentrations for both amyloid-beta (u) and tau proteins (v) and a small concentration for the astrocytes (w). Some other perturbations of these initial concentrations can change the initial propagation profiles of the concentrations, but the final results (long-term behaviours) are the same. These concentrations are uniform on all the nodes in the brain connectome. We consider the initial condition $q = 0$ for all the nodes for the damage equation. As toxic loads propagate over the brain connectome, they damage the neurons in the brain.

5.1. Primary and secondary tauopathies

As in our previous study, we have shown that the evolution profiles of both toxic loads remain the same for primary and secondary tauopathies in the absence of astrocytes [45]. Here also, we observe that their profiles remain the same for both tauopathies in the presence of astrocytes. So, without the loss of generality, we present the results for the parameter values corresponding to the secondary tauopathy. A synthetic parameter set for the secondary tauopathy is mentioned in Table 1. We also studied a more general case (mixed tauopathy) where non-uniform parameter values are considered on different nodes in the brain connectome.

Table 1: Synthetic parameter values [43].

Parameter	Value	Parameter	Value	Parameter	Value	Parameter	Value
a_0	1.035	a_1	1.38	a_2	1.38	\tilde{a}_1	0.828
b_0	0.69	b_1	1.38	b_2	1.035	\tilde{b}_1	0.552
b_3	4.14	c_0	1.0	c_1	0.1	μ	0.1
ρ_1	1.38	ρ_2	0.138	ρ_3	1.38	ρ_4	0.014
k_1	0.0001	k_2	0.01	k_3	0.1	k_4	0.001

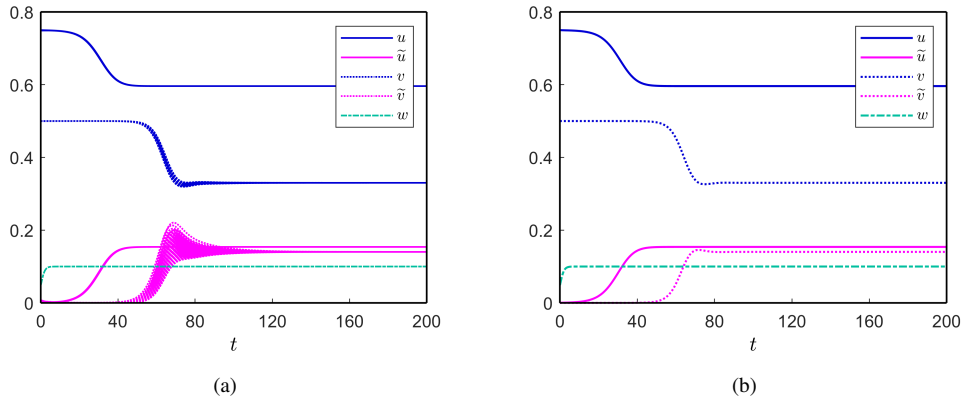


Figure 2: (Color online) Solutions for the non-fractional model of (5) in the brain connectome: (a) solutions in each region and (b) the spatial average solution. The parameter values are in Table 1.

5.1.1. Dual role of astrocytes

As we stated earlier, the astrocytes play a dual role in disease propagation. Astrocytes try to clear the toxic amyloid-beta and maintain a healthy balance in the brain. But, due to the accumulation of high concentrations of toxic amyloid-beta, astrocytes over-activate and help propagate the disease rather than save the brain from the disease. Therefore, depending on the concentrations of astrocytes present in the brain cells, two scenarios can occur: (i) astrocytes control the toxic amyloid-beta, and (ii) astrocytes can not control the toxic amyloid-beta. Here, we capture both cases through our considered network mathematical model. In our model, the parameter c_1 represents the maximum concentration (carrying capacity) of astrocytes in the brain cells. We consider two different carrying capacities for the astrocytes in the network model, and the average toxic density propagations over time are shown in Fig. 3. For $c_1 = 0.3$, with an increase in the clearance rate μ , the toxic load over the brain connectome decreases [see Fig. 3(a)]. This shows that astrocytes can control the brain's toxic loads. On the other hand, for $c_1 = 0.1$, they fail to control the healthy balance in the brain connectome, and support an increase in the toxic loads [see Fig. 3(b)].

5.1.2. Memory effect

Here, we analyze the memory effect of AD progression in the brain connectome. As mentioned earlier, the model (5) with $\alpha = 1$ corresponds to no memory and has memory for $0 < \alpha < 1$. As discussed in Sect 2, the underlying processes are non-Markovian. Figure 4 depicts both the toxic propagation over the brain connectome for no-memory and with memory. In the figure, we plot the spatial average of toxic amyloid-

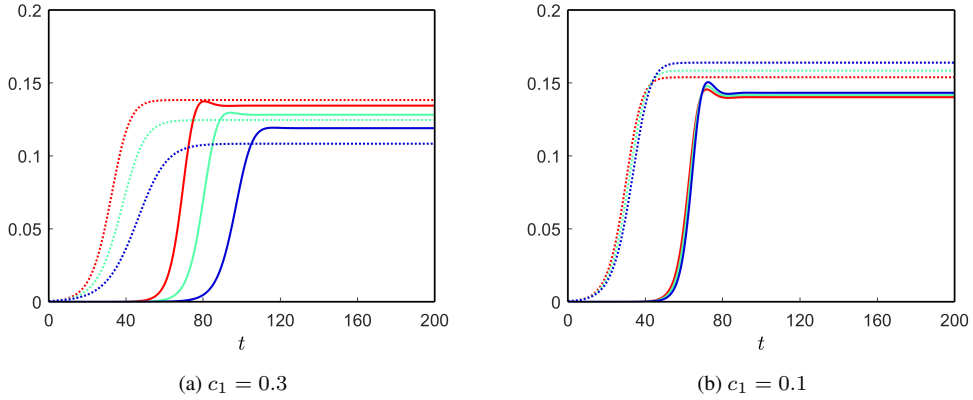


Figure 3: (Color online) Spatial average solutions of \tilde{u} (dotted) and \tilde{v} (solid) for the non-fractional model (5) for different values of c_1 and μ : $\mu = 0.1$ (red), $\mu = 0.2$ (green) and $\mu = 0.3$ (blue). The other parameter values are in Table 1.

beta and toxic tau protein. Here, the evolution time of the toxic loads for the fractional model is higher compared to the non-fractional model. Furthermore, with an increase in the memory effect (decreasing the value of α), the evolution-time of toxic loads also increases [see Fig. 4].

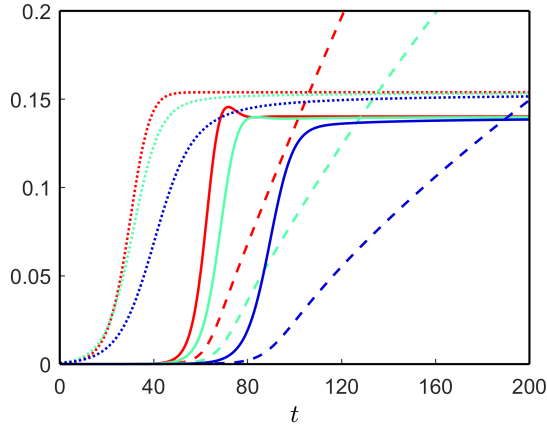


Figure 4: (Color online) Spatial average solutions of \tilde{u} (dotted), \tilde{v} (solid) and q (dashed) for the fractional model of (5) with (6) for different values of α with the other fixed parameter values of Table 1 over the brain connectome. In the plot $\alpha = 1$, $\alpha = 0.9$ and $\alpha = 0.8$ are represented by the red, green and blue curves, respectively.

5.1.3. Neuronal damage

Following the model (6), the neuronal damage depends on the toxic loads in the brain connectome; hence, the requirement depends on the evolutional time (the time required to converge to its stable steady-state) of toxic loads. We mention the parameter values directly associated with the neuronal damage in Table 1. This choice of the parameter values gives us the influence of toxic tau proteins on neural damage and also in the presence of toxic amyloid-beta [59, 60, 61, 62]. We plot the spatial average of the damage in Fig. 4, and it validates the dependency. It has been observed that the damage converges to its equilibrium point $q_* = 1$ for both fractional and non-fractional models, but the case of the fractional model takes a

longer time than the non-fractional model. Overall, memory has a pronounced effect on AD propagation.

5.2. Mixed tauopathy

Here, we focus on the disease propagation for non-uniform parameters over the brain connectome. This is more realistic than the uniform parameters as the presence of heterogeneous density of the ingredients in the brain (e.g., proteins, chemical ions, etc.). We consider the parameter values of b_2 and b_3 from Table 1 in all the brain identities (IDs) except some regions mentioned in Tables 2 and 3. Due to the non-uniform parameter values in the brain connectome, a mixture of primary and secondary tauopathies occurs in the network model, called mixed tauopathy. This causes different stable coexisting steady-states in the network model, and we divide these into two parts: region ID and region-wise disease propagation.

Table 2: Modified b_3 parameter values in different brain IDs [43].

Brain ID and modified b_3 value			
Pars opercularis	7.452	Rostral middle frontal gyrus	6.707
Superior frontal gyrus	7.452	Caudal middle frontal gyrus	7.452
Precentral gyrus	5.589	Postcentral gyrus	3.726
Lateral orbitofrontal cortex	6.486	Medial orbitofrontal cortex	6.486
Pars triangularis	5.520e-6	Rostral anterior cingulate	6.210e-6
Posterior cingulate cortex	3.45	Inferior temporal cortex	13.11
Middle temporal gyrus	11.04	Superior temporal sulcus	8.97
Superior temporal gyrus	8.28	Superior parietal lobule	12.42
Cuneus	13.8	Pericalcarine cortex	13.8
Inferior parietal lobule	11.73	Lateral occipital sulcus	15.18
Lingual gyrus	13.8	Fusiform gyrus	7.59
Parahippocampal gyrus	11.04	Temporal pole	1.104e-5

Table 3: Modified b_2 and b_3 parameter values in different brain IDs [43].

Brain ID	Entorhinal cortex	Pallidum	Locus coeruleus	Putamen	Precuneus
b_2	3.125	2.76	1.38	3.795	3.105
b_3	1.104e-5	2.76	1.38	3.795	3.105

5.2.1. Region ID-wise AD propagation

The integrated brain connectome data has forty-nine brain IDs, each containing one or more nodes. We calculate the average concentration of the toxic amyloid-beta for each brain ID by the formula [63]:

$$M_{\tilde{u}}^d = \frac{1}{n_d} \sum_{k \in \mathcal{R}_d} \tilde{u}_k, \quad (7)$$

where \mathcal{R}_d is defined as the set of all nodes in that brain ID, and n_d is the number of elements in \mathcal{R}_d . We use the same formula for the toxic tau proteins and also for the damage dynamics. For the non-fractional

model, we observe uniform average concentrations of toxic amyloid-beta (not shown here) and non-uniform average concentrations of toxic tau proteins along the brain IDs [see Fig. 5 (a)]. This happens due to the direct involvement of the non-uniform parameters b_2 and b_3 in the healthy and toxic tau proteins equations. Furthermore, the damage propagation profiles for each brain IDs are different [see Fig. 5 (b)]. According to the integrated brain connectome data, the maximum concentrations of toxic amyloid-beta accumulate in the region ID precuneus, followed by the region IDs left-putamen, right-putamen, entorhinal, and so on. The damage dynamics show that these region IDs affect the most at the initial stage of AD progression.

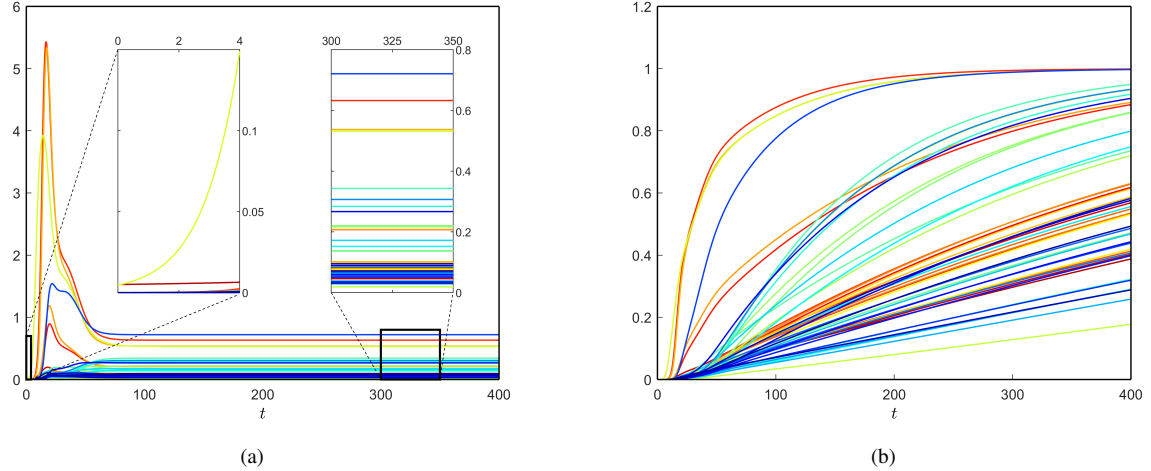


Figure 5: (Color online) Brain ID-wise average toxic tau protein (\bar{v}) propagation (a) and their damage (b) for the non-fractional model. Here, we choose the fixed parameter values $\mu = 0.2$, $c_1 = 0.3$ and others from Table 1 for all the nodes in the brain connectome except the nodes listed in Tables 2 and 3.

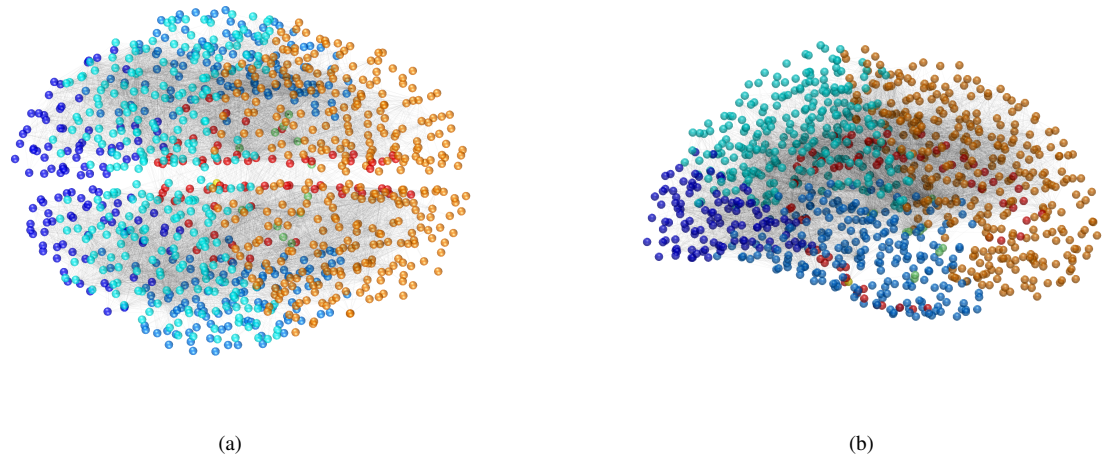


Figure 6: (Color online) Three-dimensional views of the brain with its different regions: (a) axial view and (b) sagittal view.

5.2.2. Region-wise AD propagation

Now we focus on the evolution of the toxic load distributions and their damage profile for seven brain regions (limbic, frontal, basal ganglia, parietal, temporal, occipital, and brain stem), and each region containing one or more brain IDs. We plot all the nodes lying in the mentioned regions in the brain connectome in Fig. 6. Here, different colors of the nodes belonging to different regions and their color codes are mentioned in legends in Fig. 7.

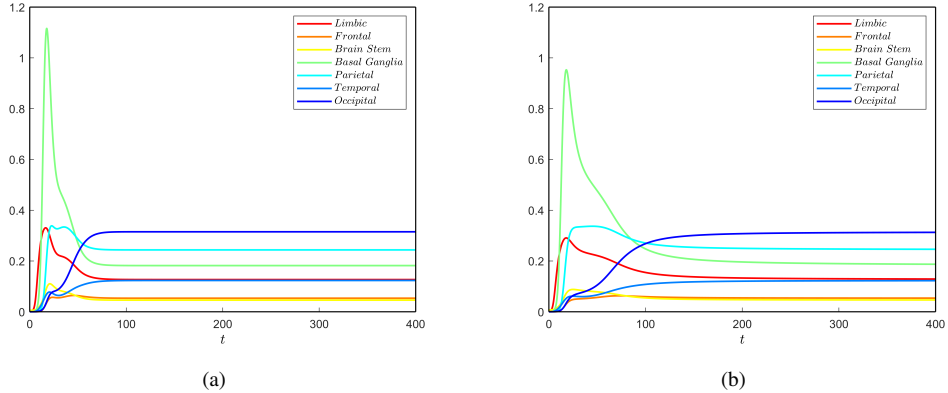


Figure 7: (Color online) Brain region-wise average toxic tau protein (\tilde{v}) propagation: (a) non-fractional model and (b) fractional model with $\alpha = 0.8$. Here, we choose the fixed parameter values $\mu = 0.2$, $c_1 = 0.3$ and others from Table 1 for all the nodes in the brain connectome except the nodes listed in Tables 2 and 3.

We apply the formula (7) to find the average toxic loads for all regions. In this case, the summation is taken over the nodes belonging to the respective regions. We plot the toxic load corresponding to tau protein for each region in Fig. 7. Due to the non-uniform parameter set in the tau protein equation, the toxic load converges to different concentrations over the regions. According to the integrated data, the occipital region accumulates the most toxic concentration, followed by the parietal, basal ganglia, limbic, temporal, frontal, and brain stem. Moreover, the toxic propagation profile for each region is different. Some regions accumulate more toxic tau protein concentration after the initial development of the disease but settle down to a comparatively lower concentration for a longer time, e.g., basal ganglia, parietal, and limbic. For the other regions, there is not much accumulation in the concentration after the starting of the disease rather, they slowly accumulate the toxic loads and help in the disease propagation. Figures 7(a) and (b) represent the toxic tau protein propagation in regions for the non-fractional model and fractional model with $\alpha = 0.8$, respectively (other parameters are mentioned in the caption and Tables 1, 2 and 3). This comparison shows that the memory effect helps in slowing down the propagation speed in the brain regions.

We apply the same formula (7) to find the regions' average damage profile. Due to the non-uniform distributions of the toxic tau proteins, the damage profile for each region is different. The region corresponding to the maximum toxic concentration is damaged first, then the region with the second-highest concentration, and so on. Figure 8 shows the neuronal damage propagation for both non-fractional and fractional models. In the results, the damage dynamics are shown till $t = 400$ (non-dimensional time), but we observe that the required time to damage each region in the brain for the fractional model is higher compared to the non-fractional model. Hence, the memory effect takes a longer time to damage the brain cell.

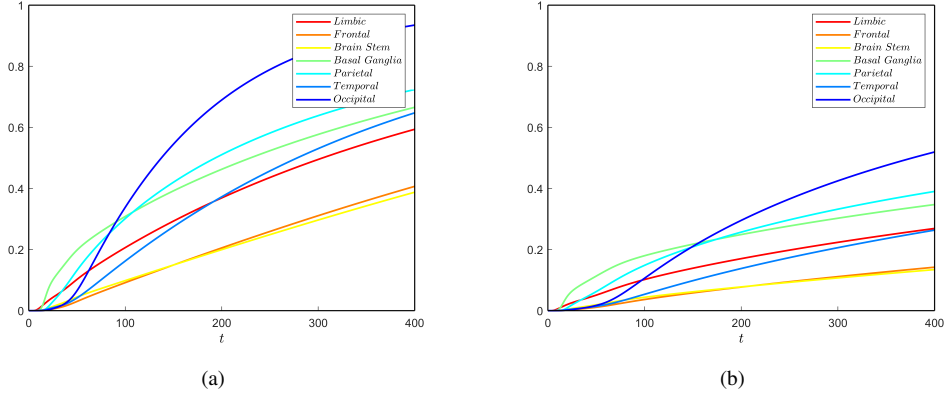


Figure 8: (Color online) Brain region-wise average damage propagation: (a) non-fractional model and (b) fractional model with $\alpha = 0.8$. Here, we choose the fixed parameter values $\mu = 0.2$, $c_1 = 0.3$ and Table 1 for all the nodes in the brain connectome except the nodes listed in Tables 2 and 3.

6. Summary

In this work, we have considered a modified heterodimer model for protein-protein interactions for each of the proteins ($A\beta$ and τP), accounting for their coupling. We incorporated the coupled dynamics of astrocytes dynamics into the modified model and studied the dual role of astroglia before and after AD. Furthermore, we have studied the memory effect in AD progression, which is highly relevant to disease progression. Most of these investigations have been carried out by considering the heterogeneous parameter values, and it is a more realistic synthetic parameter set-up.

Depending on the presence of astrocytes, the considered network model shows the dual behaviour in the disease propagation. For higher astrocytes' densities, the density corresponding to the toxic amyloid-beta increases with an increase in its clearance rate by astrocytes. On the other hand, for smaller astrocytes' densities, the opposite scenario holds. Therefore, if a sufficient amount of astrocytes is present in the brain, they can minimize or delay AD development; otherwise, they help in AD propagation. Furthermore, the fractional differential derivative framework presented here helps to model the memory effect on AD progression. We have shown that an increase in memory (by decreasing the parameter values α) causes a delay in the toxic density propagations in the brain. As a result, it slows down the AD development in the brain.

We have studied the network model for the parameter values where conditions of primary and secondary tauopathies are satisfied in different brain regions. This causes a non-homogeneous distribution of toxic tau proteins in the brain. Furthermore, different neuronal damage profiles are shown on different brain IDs and also in different brain regions. Therefore, heterogeneous parameter values in the network model capture a realistic scenario of AD progression in the brain. The coupling of astrocytes to $A\beta$ and τP represents an advancement in this direction. Along with the memory, considering heterogeneous parameter values corresponding to amyloid-beta or astrocytes in different brain IDs or regions is an important avenue for future research on this model.

Acknowledgements

The authors are grateful to the NSERC and the CRC Program for their support. RM also acknowledges the support of the BERC 2022–2025 program and the Spanish Ministry of Science, Innovation and Universities through the Agencia Estatal de Investigacion (AEI) BCAM Severo Ochoa excellence accreditation SEV-2017-0718 and the Basque Government fund AI in BCAM EXP. 2019/00432. This research was enabled in part by support provided by SHARCNET (www.sharcnet.ca) and Digital Research Alliance of Canada (www.alliancecan.ca).

References

- [1] A. Alzheimer, Über einen eigenartigen schweren erkrankungsprozeß der hirnrinde., *Neurol Central.* 25 (1906) 1134.
- [2] H. Möller, M. Graeber, The case described by Alois Alzheimer 1911, *Eur. Arch Psychiatry Clin Neurosci.* 248 (1998) 111–127.
- [3] H. Hippius, G. Neundörfer, The discovery of Alzheimer's disease, *Dialogues Clin Neurosci.* 5 (2003) 101–108.
- [4] D. Harman, Alzheimer's disease pathogenesis: role of aging, *Annals of the New York Academy of Sciences* 1067 (1) (2006) 454–460.
- [5] R. Sengoku, Aging and Alzheimer's disease pathology, *Neuropathology* 40 (1) (2020) 22–29.
- [6] E. Bagyinszky, Y. C. Youn, S. S. A. An, S. Kim, The genetics of Alzheimer's disease, *Clinical interventions in aging* 9 (2014) 535.
- [7] G. T. Grossberg, Diagnosis and treatment of Alzheimer's disease, *Journal of Clinical Psychiatry* 64 (2003) 3–6.
- [8] M. F. Weiner, L. Hynan, M. Bret, C. White Iii, Early behavioral symptoms and course of Alzheimer's disease, *Acta Psychiatrica Scandinavica* 111 (5) (2005) 367–371.
- [9] J. Sevigny, P. Chiao, T. Bussière, P. H. Weinreb, L. Williams, M. Maier, R. Dunstan, S. Salloway, T. Chen, Y. Ling, et al., The antibody aducanumab reduces A β plaques in Alzheimer's disease, *Nature* 537 (7618) (2016) 50–56.
- [10] D. J. Selkoe, Alzheimer disease and aducanumab: adjusting our approach, *Nature Reviews Neurology* 15 (7) (2019) 365–366.
- [11] R. Howard, K. Y. Liu, Questions emerge as biogen claims aducanumab turnaround, *Nature Reviews Neurology* 16 (2) (2020) 63–64.
- [12] M. Murpy, H. LeVine III, Alzheimer's disease and the β -amyloid peptide, *J Alzheimers Dis* 19 (1) (2010) 311–323.
- [13] G. K. Gouras, T. T. Olsson, O. Hansson, β -amyloid peptides and amyloid plaques in Alzheimer's disease, *Neurotherapeutics* 12 (1) (2015) 3–11.
- [14] C. Liu, The role of mesenchymal stem cells in regulating astrocytes-related synapse dysfunction in early Alzheimer's disease, *Frontiers in Neuroscience* 16 (2022) 927256.
- [15] E. B. Rischel, M. Gejl, B. Brock, J. Rungby, A. Gjedde, In Alzheimer's disease, amyloid beta accumulation is a protective mechanism that ultimately fails, *Alzheimer's & dementia: the journal of the Alzheimer's Association* (2022).
- [16] A. R. Roda, G. Serra-Mir, L. Montoliu-Gaya, L. Tiessler, S. Villegas, Amyloid-beta peptide and tau protein crosstalk in Alzheimer's disease, *Neural Regeneration Research* 17 (8) (2022) 1666.
- [17] X. Sun, W.-D. Chen, Y.-D. Wang, β -amyloid: the key peptide in the pathogenesis of Alzheimer's disease, *Frontiers in pharmacology* 6 (2015) 221.
- [18] D. Burdick, B. Soreghan, M. Kwon, J. Kosmoski, M. Knauer, A. Henschen, J. Yates, C. Cotman, C. Glabe, Assembly and aggregation properties of synthetic Alzheimer's A4/beta amyloid peptide analogs, *Journal of Biological Chemistry* 267 (1) (1992) 546–554.
- [19] S. A. Gravina, L. Ho, C. B. Eckman, K. E. Long, L. Otvos, L. H. Younkin, N. Suzuki, S. G. Younkin, Amyloid β protein (a β) in Alzheimer's disease brain: Biochemical and immunocytochemical analysis with antibodies specific for forms ending at a β 40 or a β 42 (43), *Journal of Biological Chemistry* 270 (13) (1995) 7013–7016.
- [20] J. Kim, L. Onstead, S. Randle, R. Price, L. Smithson, C. Zwizinski, D. W. Dickson, T. Golde, E. McGowan, A β 40 inhibits amyloid deposition in vivo, *Journal of Neuroscience* 27 (3) (2007) 627–633.
- [21] R. Medeiros, D. Baglietto-Vargas, F. M. LaFerla, The role of tau in Alzheimer's disease and related disorders, *CNS neuroscience & therapeutics* 17 (5) (2011) 514–524.
- [22] S. Muralidhar, S. V. Ambi, S. Sekaran, D. Thirumalai, B. Palaniappan, Role of tau protein in Alzheimer's disease: The prime pathological player, *International journal of biological macromolecules* 163 (2020) 1599–1617.
- [23] T. Guo, W. Noble, D. P. Hanger, Roles of tau protein in health and disease, *Acta neuropathologica* 133 (5) (2017) 665–704.
- [24] R. B. Kargbo, Treatment of Alzheimer's by PROTAC-Tau protein degradation (2019).

[25] S. Illenberger, Q. Zheng-Fischhofer, U. Preuss, K. Stamer, K. Baumann, B. Trinczek, J. Biernat, R. Godemann, E.-M. Mandelkow, E. Mandelkow, The endogenous and cell cycle-dependent phosphorylation of tau protein in living cells: implications for Alzheimer's disease, *Molecular biology of the cell* 9 (6) (1998) 1495–1512.

[26] K. A. Johnson, S. Minoshima, N. I. Bohnen, K. J. Donohoe, N. L. Foster, P. Herscovitch, J. H. Karlawish, C. C. Rowe, M. C. Carrillo, D. M. Hartley, et al., Appropriate use criteria for amyloid PET: a report of the amyloid imaging task force, the society of nuclear medicine and molecular imaging, and the Alzheimer's association, *Alzheimer's & Dementia* 9 (1) (2013) E1–E16.

[27] M. Grundman, K. A. Johnson, M. Lu, A. Siderowf, A. K. Arora, D. M. Skovronsky, M. A. Mintun, M. J. Pontecorvo, et al., Effect of amyloid imaging on the diagnosis and management of patients with cognitive decline: impact of appropriate use criteria, *Dementia and geriatric cognitive disorders* 41 (1-2) (2016) 80–92.

[28] G. D. Rabinovici, C. Gatsonis, C. Apgar, K. Chaudhary, I. Gareen, L. Hanna, J. Hendrix, B. E. Hillner, C. Olson, O. H. Lesman-Segev, et al., Association of amyloid positron emission tomography with subsequent change in clinical management among medicare beneficiaries with mild cognitive impairment or dementia, *Jama* 321 (13) (2019) 1286–1294.

[29] M. D. Devous, A. D. Joshi, M. Navitsky, S. Southeikal, M. J. Pontecorvo, H. Shen, M. Lu, W. R. Shankle, J. P. Seibyl, K. Marek, et al., Test-retest reproducibility for the tau PET imaging agent Flortaucipir F 18, *Journal of Nuclear Medicine* 59 (6) (2018) 937–943.

[30] M. D. Devous Sr, A. S. Fleisher, M. J. Pontecorvo, M. Lu, A. Siderowf, M. Navitsky, I. Kennedy, S. Southeikal, T. S. Harris, M. A. Mintun, Relationships between cognition and neuropathological tau in Alzheimer's disease assessed by 18F Flortaucipir PET, *Journal of Alzheimer's Disease* 80 (3) (2021) 1091–1104.

[31] N. J. Abbott, L. Rönnbäck, E. Hansson, Astrocyte-endothelial interactions at the blood-brain barrier, *Nature reviews neuroscience* 7 (1) (2006) 41–53.

[32] C. Eroglu, B. A. Barres, Regulation of synaptic connectivity by glia, *Nature* 468 (7321) (2010) 223–231.

[33] K. Hayakawa, E. Esposito, X. Wang, Y. Terasaki, Y. Liu, C. Xing, X. Ji, E. H. Lo, Transfer of mitochondria from astrocytes to neurons after stroke, *Nature* 535 (7613) (2016) 551–555.

[34] Y. Kim, J. Park, Y. K. Choi, The role of astrocytes in the central nervous system focused on bk channel and heme oxygenase metabolites: a review, *Antioxidants* 8 (5) (2019) 121.

[35] O. E. Tasdemir-Yilmaz, M. R. Freeman, Astrocytes engage unique molecular programs to engulf pruned neuronal debris from distinct subsets of neurons, *Genes & development* 28 (1) (2014) 20–33.

[36] S. Koizumi, Y. Hirayama, Y. M. Morizawa, New roles of reactive astrocytes in the brain: an organizer of cerebral ischemia, *Neurochemistry international* 119 (2018) 107–114.

[37] S. Pal, R. Melnik, The role of astrocytes in Alzheimer's disease progression, in: I. Rojas, O. Valenzuela, F. Rojas, L. J. Herrera, F. Ortúño (Eds.), *Bioinformatics and Biomedical Engineering*, Springer, 2022, pp. 47–58.

[38] M. Yuan, H. Wu, Astrocytes in the traumatic brain injury: the good and the bad, *Experimental Neurology* 348 (2022) 113943.

[39] C. Garwood, L. Ratcliffe, J. Simpson, P. Heath, P. Ince, S. Wharton, astrocytes in Alzheimer's disease and other age-associated dementias: a supporting player with a central role, *Neuropathology and Applied Neurobiology* 43 (4) (2017) 281–298.

[40] A. Y. Abramov, M. R. Duchen, The role of an astrocytic NADPH oxidase in the neurotoxicity of amyloid beta peptides, *Philosophical Transactions of the Royal Society B: Biological Sciences* 360 (1464) (2005) 2309–2314.

[41] Y. S. Kim, H. M. Jung, B.-E. Yoon, Exploring glia to better understand Alzheimer's disease, *Animal cells and systems* 22 (4) (2018) 213–218.

[42] C.-C. Liu, N. Zhao, Y. Fu, N. Wang, C. Linares, C.-W. Tsai, G. Bu, ApoE4 accelerates early seeding of amyloid pathology, *Neuron* 96 (5) (2017) 1024–1032.

[43] T. B. Thompson, P. Chaggar, E. Kuhl, A. Goriely, A. D. N. Initiative, Protein-protein interactions in neurodegenerative diseases: A conspiracy theory, *PLoS computational biology* 16 (10) (2020) e1008267.

[44] G. Meisl, E. Hidari, K. Allinson, T. Rittman, S. L. DeVos, J. S. Sanchez, C. K. Xu, K. E. Duff, K. A. Johnson, J. B. Rowe, et al., In vivo rate-determining steps of tau seed accumulation in Alzheimer's disease, *Science advances* 7 (44) (2021) eabh1448.

[45] S. Pal, R. Melnik, Nonlocal models in the analysis of brain neurodegenerative protein dynamics with application to Alzheimer's disease, *Scientific Reports* 12 (1) (2022) 1–13.

[46] M. T. Tacconi, Neuronal death: is there a role for astrocytes?, *Neurochemical research* 23 (5) (1998) 759–765.

[47] D. R. Thal, The role of astrocytes in amyloid β -protein toxicity and clearance, *Experimental neurology* 236 (1) (2012) 1–5.

[48] A. Stanislavsky, Memory effects and macroscopic manifestation of randomness, *Physical Review E* 61 (5) (2000) 4752.

[49] J. Cressoni, G. Viswanathan, A. Ferreira, M. da Silva, Alzheimer random walk model: two previously overlooked diffusion regimes, *Physical Review E* 86 (4) (2012) 042101.

[50] J. Cressoni, L. Da Silva, G. Viswanathan, M. Da Silva, Robustness of the non-Markovian Alzheimer walk under stochastic perturbation, *EPL (Europhysics Letters)* 100 (6) (2013) 60003.

[51] M. Saeedian, M. Khalighi, N. Azimi-Tafreshi, G. Jafari, M. Ausloos, Memory effects on epidemic evolution: The susceptible-infected-recovered epidemic model, *Physical Review E* 95 (2) (2017) 022409.

[52] M. I. Troparevsky, S. A. Seminara, M. A. Fabio, A review on fractional differential equations and a numerical method to solve some boundary value problems, *Nonlinear Systems-Theoretical Aspects and Recent Applications* (2019).

[53] M. Mohammad, A. Trounev, Explicit tight frames for simulating a new system of fractional nonlinear partial differential equation model of Alzheimer disease, *Results in Physics* 21 (2021) 103809.

[54] A. R. Carvalho, C. Pinto, D. Baleanu, HIV/HCV coinfection model: a fractional-order perspective for the effect of the HIV viral load, *Advances in Difference Equations* 2018 (1) (2018) 1–22.

[55] U. Ghosh, S. Pal, M. Banerjee, Memory effect on Bazykin's prey-predator model: Stability and bifurcation analysis, *Chaos, Solitons & Fractals* 143 (2021) 110531.

[56] R. Thuraisingham, A kinetic scheme to examine the role of glial cells in the pathogenesis of Alzheimer's disease, *Metabolic Brain Disease* (2022) 1–5.

[57] C. Kerepesi, B. Szalkai, B. Varga, V. Grolmusz, How to direct the edges of the connectomes: Dynamics of the consensus connectomes and the development of the connections in the human brain, *Plos one* 11 (6) (2016) e0158680.

[58] B. Szalkai, C. Kerepesi, B. Varga, V. Grolmusz, High-resolution directed human connectomes and the consensus connectome dynamics, *Plos one* 14 (4) (2019) e0215473.

[59] S. A. Small, K. Duff, Linking $\alpha\beta$ and tau in late-onset Alzheimer's disease: a dual pathway hypothesis, *Neuron* 60 (4) (2008) 534–542.

[60] A. Lloret, M.-C. Badia, E. Giraldo, G. Ermak, M.-D. Alonso, F. V. Pallardó, K. J. Davies, J. Viña, Amyloid- β toxicity and tau hyperphosphorylation are linked via RCAN1 in Alzheimer's disease, *Journal of Alzheimer's Disease* 27 (4) (2011) 701–709.

[61] H. Cho, J. Y. Choi, M. S. Hwang, Y. J. Kim, H. M. Lee, H. S. Lee, J. H. Lee, Y. H. Ryu, M. S. Lee, C. H. Lyoo, In vivo cortical spreading pattern of tau and amyloid in the Alzheimer disease spectrum, *Annals of neurology* 80 (2) (2016) 247–258.

[62] C. R. Jack Jr, D. A. Bennett, K. Blennow, M. C. Carrillo, B. Dunn, S. B. Haeberlein, D. M. Holtzman, W. Jagust, F. Jessen, J. Karlawish, et al., NIA-AA research framework: toward a biological definition of Alzheimer's disease, *Alzheimer's & Dementia* 14 (4) (2018) 535–562.

[63] S. Fornari, A. Schäfer, E. Kuhl, A. Goriely, Spatially-extended nucleation-aggregation-fragmentation models for the dynamics of prion-like neurodegenerative protein-spreading in the brain and its connectome, *Journal of theoretical biology* 486 (2020) 110102.